

RESEARCH ARTICLE

Open Access



# Radiomics Feature Extraction from Ultrasound B-Mode Images and Radio-Frequency Signals of the Carotid Arterial Wall: A Feasibility Study

Maryam Jadoon<sup>1\*</sup>, Federica Poli<sup>1</sup>, Pierre Boutouyrie<sup>1,2</sup>, Hakim Khettab<sup>2</sup>, Elisabetta Bianchini<sup>3</sup>, Francesco Faita<sup>3</sup>, Xavier Jouven<sup>1</sup>, Jean Philippe Empana<sup>1†</sup> and Rosa Maria Bruno<sup>1,2†</sup>

## Abstract

**Background** Carotid ultrasound is largely used to assess arterial aging. Radiomics (quantitative imaging feature analysis) applied on ultrasound may allow characterizing wall ultrastructure and arterial ageing. However, to date its application to the intima–media (IM) complex is unexplored. The aim of this study is to investigate the feasibility of radiomics-based B-mode and RF feature extraction and selection process.

**Methods** Radio-frequency signals from 200 individuals (age 50–75y, 40% hypertensives, 20% diabetic) were used to extract RF and B-mode features. Feature stability across three frames from the same clip and five ROI sizes for each frame were evaluated by intraclass correlation analysis (threshold > 0.50). Lasso L1 regression for chronological age prediction on ICC > 0.50 features were used to analyze reproducibility and variation across frames and ROI sizes; 80/20 train-test split was used, with performance evaluated by MSE and  $R^2$ .

**Results** Radiomic feature extraction was feasible in 190 among 200 individuals. 48 features showed an ICC > 0.50. Feature selection for chronological age prediction showed consistent  $R^2$  (0.09–0.14 train, 0.05–0.13 test) and MSE (32.3–34.3 train, 30.7–42.3 test) across frames. Fixed ROI sizes of 1.0mm and 1.2mm had comparable performance to an ROI size manually tailored to wall thickness:  $R^2$  (0.07–0.15 train, 0.07–0.17 test) and MSE (33.15–36.22 train, 33.07–34.83 test), consistently selecting substantially similar three to six features.

**Conclusion** While feature extraction and selection process are largely reproducible across frames, ROI size proved critical and thus must be carefully chosen. Further studies are required to demonstrate the validity of this approach for carotid wall characterization.

**Keywords** Vascular aging, Carotid radiomics, Arterial stiffness, Radio-frequency ultrasound, Machine learning

<sup>†</sup>Jean Philippe Empana and Rosa Maria Bruno have contributed equally to this paper.

\*Correspondence:

Maryam Jadoon

Maryam13khan@gmail.com

Full list of author information is available at the end of the article



## 1 Introduction

Vascular ageing is marked by progressive structural and functional deterioration of blood vessels that occurs with ageing. These changes over time increase the risk of developing cardiovascular disease [1, 2]. Vascular ageing is an inevitable physiological process; however, the rate and extent of this vascular deterioration can vary considerably among certain individuals. Early vascular ageing (EVA) exhibits structural and functional arterial changes typically associated with older age, despite being chronologically younger [3, 4]. Conversely, in supernormal vascular ageing (SUPERNOVA), individuals demonstrate remarkable preservation of vascular health and function, with their arteries appearing physiologically younger than their chronological age. In recent years, there has been an increased evidence on the role of vascular ageing biomarkers in predicting cardiovascular events [5, 6].

The current assessment of vascular ageing may involve utilizing biomarkers for atherosclerosis, such as the calcium score (CAC) or plaque analysis, as well as biomarkers for arteriosclerosis, including pulse wave velocity (PWV) and carotid distensibility [7]. These image-based assessments are typically performed using various imaging techniques, including magnetic resonance imaging (MRI), computed tomography (CT), and ultrasound (US). Thorough evaluations of both structural and functional vascular alterations are essential for assessing the cardiovascular risk associated with vascular ageing [8]. Advanced imaging modalities such as MRI and CT, while effective, are expensive, complex and have low availability, thus not perfectly suitable for routine preventive risk assessments. In contrast, carotid US assessment is relatively low cost, safe, widely available and able to capture both atherosclerotic and arteriosclerotic biomarkers. This makes it an optimal choice for routine preventive risk assessment. Among carotid ultrasound biomarkers, carotid plaque [9, 10] and carotid stiffness [11] demonstrated predictive value for cardiovascular events, mostly stroke, on top of cardiovascular risk factors [12]. Conversely Intima-media thickness (IMT) additive predictive value is debated: while IMT is associated with cardiovascular risk factors and is useful for understanding response to treatment [13], its ability to enhance risk prediction beyond existing methods is limited [14]. For this reason, there is a need for continuous improvement of methods and techniques aimed at developing new descriptors, to better capture the subtle structural variations in the carotid arteries [8, 15]. It is now well documented that radiomics, which involves extracting numerical data from images, can provide more detailed information than simple images and in some settings can be comparable to diagnostic assessment by radiologists [16, 17]. Multiple studies have validated the predictive

power of radiomic features (quantitative information mostly from CT or MRI images) and correlating these with clinical outcomes [16]. Especially, radiomics has proven impactful in oncology, in survival prediction for oesophageal cancer patients [18], in predicting breast cancer heterogeneity [19] and in assessing both tumour recurrence [20] and disease-free survival in advanced rectal cancer [21]. Cardiovascular applications of radiomics have also shown promise, mostly applied on coronary CT scans [22, 23], but also on carotid plaque US [24]. For example, Huang et al. explored the relationship between radiomic plaque features and clinical symptoms [25], while Le et al. assessed CT angiography radiomics for stroke prediction [26]. Liu et al. developed a radiomics nomogram for stroke risk in diabetes [27], and Van Engelen et al. demonstrated that plaque texture radiomics could predict vascular events [28]. To date, the carotid IM complex has never been investigated by radiomics, because of small tissue region size, rendering difficult feature extraction from standard B-mode images [29]. However, a more comprehensive analysis of IMT ultrastructure may provide additional information on atherosclerosis development at an earlier stage of disease, before plaque development. Indeed, lower ultrasound resolution makes it difficult to capture histological details such as cells [30, 31]. However, the integration of B-mode imaging with radio-frequency phase-derived information, alongside advanced texture analysis techniques (on both RF-B-mode), offers a promising solution to extract and quantify information about structural disarray as a consequence of cell and extracellular matrix changes [32]. We hypothesized that combining B-mode with radio-frequency (RF) signal radiomic analysis would provide complementary information for comprehensive characterization of the intima-media complex. B-mode imaging offers greyscale representation of tissue acoustic properties, morphological information and interface detection, while RF signals provide raw acoustic data with preserved phase information, higher axial sensitivity and greater spatial resolution [33]. In this study, we aimed to evaluate the feasibility of radiomics-based B-mode and RF feature extraction from the IM complex. A key focus was to assess the impact of the selected region-of-interest (ROI) size and the frame used on the extracted radiomic features.

## 2 Materials and Methods

### 2.1 Study Population

A feasibility study on a subset of 200 individuals selected from the Paris Prospective Study III (PPS3) cohort was conducted. A targeted sampling approach was implemented, oversampling individuals with type 2 diabetes (T2D) by up to 20% to capture more extreme phenotypes

associated with the condition. Additionally, the presence of carotid plaques in approximately 20% of the sample was enforced, ensuring representation of vascular complications relevant to T2D. To ensure a comprehensive range of blood pressure values, the population was divided into thirds: one-third within the 25th–75th percentile range (120–141 mmHg), one-third below the 25th percentile (< 120 mmHg), and one-third above the 75th percentile ( $\geq$  141 mmHg). Furthermore, individuals aged between 50 and 75 years were uniformly included, ensuring a consistent distribution across the age range.

PPS3 is an ongoing community-based prospective observational study conducted in Paris, France [34]. The study protocol was approved by the Ethics Committee of Cochin Hospital (Paris, France) and was registered on the World Health Organization International Clinical Trials Registry platform (NCT00741728) on 08/25/2008. A total of 10,157 men and women aged 50–75 years were enrolled, who underwent a comprehensive preventive medical checkup, after signing an informed consent form.

## 2.2 Ultrasound Acquisition

The vascular US was performed using Esaote PICUS Machine, Genova, Italy (128 RF linear array transducer with 7.5MHz, B-mode pixels 758×508 and RF-matrix 1516×127). The raw radio-frequency data were preserved to facilitate in-depth analysis. The inclusion criteria required the visibility of the intima–blood interface in at least some part of the far wall of the right common carotid artery, in a clear reconstructed B-mode image. Further details are available in the publication by PPS3 study group et al. [34].

## 2.3 Ultrasound Data Processing

First, we developed a graphical user interface (GUI) using MATLAB software (MathWorks, Inc., Massachusetts, USA, version 2022b) to process raw radio-frequency signals and to reconstruct and process B-mode images. Additionally, we identified 178 radiomics features (see description below) to be calculated from the selected region of interest (ROI). Building on previous work [35], RF signals were transformed into B-mode ultrasound images using standard techniques.

## 2.4 Radiomic Features

A total of 74 radiomic B-mode features and 104 radiomic radio-frequency (RF) features were evaluated with the GUI. The B-mode features encompassed the following: (1) first-order statistics [36], (2) higher-order textural features [37–39] (3), transform-based wavelet features [40] and (4) fractal analysis features [41, 42]. Similarly, the RF features comprised the following [43]: (1) time series

features computed individually for each RF time series within the region of interest (ROI), with the mean value computed on 30 frames to derive the time domain characteristics [44]; (2) frequency domain features involving Fourier transform to acquire the frequency spectrum, followed by straight-line fitting on the normalized spectrum [45, 46]; furthermore, (3) the M parameter extracted from the Nakagami distribution mean diagram (NDM) parametric map [45, 47] utilizing Nakagami distribution; (4) spectral features [46]; (5) the calculated feature maps such as direct energy attenuation diagram (DEA) and RF signal skewness intensity diagram (RF-I), and the first-order statistics and higher-order textural features extracted from each map by applying the texture analysis [45, 48] (Table 1).

## 2.5 Data Extraction Settings

180 B-mode images (frames) were obtained from every original 6-s acquisition (a 128 radio-frequency line multi-array with a depth of 4 cm captured at 30 frames per second). The region of interest was manually selected from the B-mode image capturing the intima–media complex on the far wall of the right carotid artery using a rectangular bounding box. Three end-diastolic frames from each patient were selected. For each frame, four ROI sizes (1 mm, 1.2 mm, 1.4 mm, and 1.6 mm) were extracted from the same location, with the bounding box centred on the smoothest section of the far wall to ensure optimal visualization of the Intima–blood interface (as depicted in Fig. 1). The bounding box encompassed the blood intima interface with minimal blood lumen on one side and the adventitia on the other. Initially, the bounding box was set at 1mm, gradually expanding by 0.2 mm towards the adventitia side while maintaining its position, to obtain the four different ROI sizes. Additionally, a fifth ROI size, termed the variable ROI, was introduced, which is the most suitable size among the four, precisely covering the intima–media (IM) complex (visually selected). Once extracted with the GUI, the features were normalized before performing feature selection.

## 2.6 Statistical Analysis and Feature Engineering

Descriptive statistics for population variables are presented as mean  $\pm$  standard deviation (SD) or as counts ( $n$ ) and percentages (%). First, we evaluated the feature stability across the three frames of the same clip and five ROI sizes of each frame by applying intraclass correlation (ICC) analysis with threshold of  $ICC > 0.50$ . We applied a two-way mixed effects model to calculate absolute agreement, treating ROI sizes as fixed effects and individuals as random effects [44]. Second, we investigated the impact of frame variability on the subset of extracted features with  $ICC > 0.50$  using the

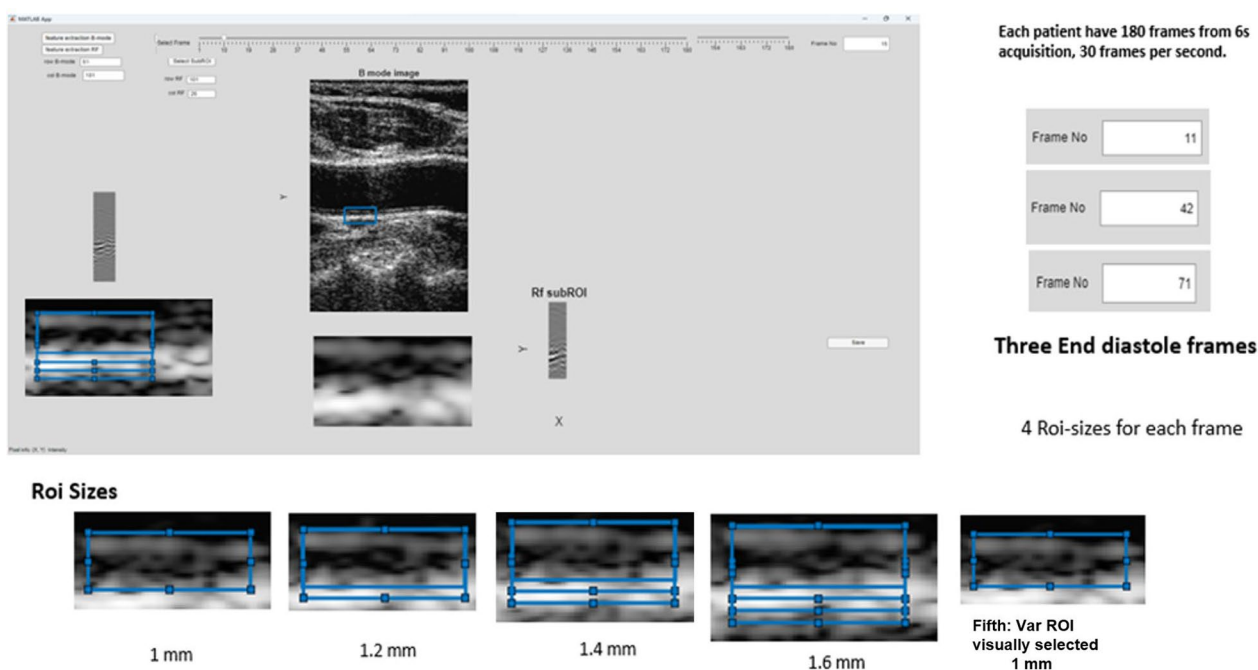


**Fig. 1** Graphical User Interface for ultrasound image visualization, ROI selection and feature extraction

feature selection technique. We applied least absolute shrinkage and selection operator (Lasso—L1 regularization) with chronological age as outcome [49]. The following metrics were compared: number, type of selected features, mean square error (MSE) and  $R^2$ . These metrics were calculated from four datasets: the three containing the features extracted by three selected frames and one containing their median values, using the variable ROI size. Internal validation was tested by 80/20 split sample technique.

Thirdly, the impact of variation in ROI size on the subset of extracted features with  $ICC > 0.50$  was also investigated by Lasso L1 regression. The following metrics were compared: number, type of selected features, MSE and  $R^2$ . These metrics were calculated from the five datasets containing the median value of each feature for the three frames for five ROI sizes (1.0 mm, 1.2 mm, 1.4 mm, 1.6 mm and Var ROI). The internal validation was tested by the 80/20 split sample technique. Additionally, we performed sensitivity analyses by applying minimum redundancy maximum relevance (MRMR) and stepwise feature selection methods instead of Lasso L1, to validate the stability and reproducibility of the results with other feature selection techniques (see workflow diagram Fig. 2). The analyses were carried out using RStudio version 2023.9.0.463 (Boston, MA), utilizing glmnet, mlr, caret, dplyr, mRMRe, e1071 and tidyverse packages.

### 3 Results

#### 3.1 Characteristics of the Study Population

Out of the initial cohort of 200 individuals, 10 were excluded because the reconstructed images did not display clearly the IMT complex in any frame, and thus the analysis was run in 190 individuals. There were 48.42% (92) women, 40% (77) hypertensives, 15.78% (30) with the presence of carotid plaques and 20% (37) diabetic individuals, with a mean IMT of  $631 \mu\text{m} \pm 108$  standard deviation (std) and mean age of 59.47 years (Max 74.07—Min 50.01). The baseline characteristics of the study population are mentioned in Table 2 and the carotid geometric and mechanical properties are mentioned in Table 3.

#### 3.2 Feature Stability Across the Frames

Features showing  $ICC > 0.50$  were 73 when ROI size was 1 mm, 72 when ROI size was 1.2 mm, 65 when ROI size was 1.4 mm, 60 when ROI size was 1.6 mm and the variable ROI (which was used as a reference) yielded 48 features. Notably, all 48 features with  $ICC > 0.50$  when ROI size was variable were also part of the sets identified by the fixed ROI sizes (See Table S1 in the Supplementary file). These features included 40 B-mode features (5 first-order, 21 higher-order, 9 wavelet transform features) and 8 RF features (5 first-order and 3 time series features).

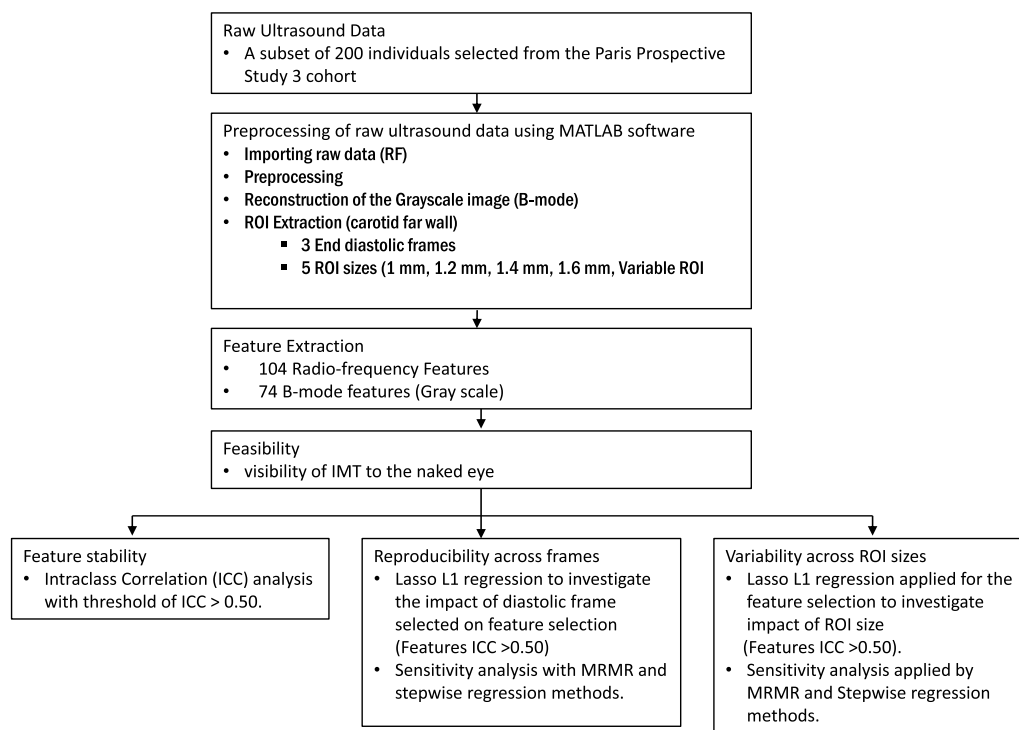


**Fig. 2** Comprehensive workflow for radiomics-based analysis of vascular ageing using b-mode and radiofrequency ultrasound imaging of the right common carotid artery

### 3.3 Reproducibility of Features Across Frames

Selected features varied in number from two to ten, but feature type and class were similar across frames. Selected features included B-mode first-order and higher-order features, as well as RF first-order features (Table 4). L1 regularization demonstrated consistent  $R^2$  (0.09–0.14 in the train set, 0.05–0.13 in the test set) and mean square error values (32.3–34.3 in the train set, 30.7–42.3 in the test set) across the four datasets. Similar and consistent model performance was observed with different feature selection models (MRMR and stepwise regression, in Table S2 of Supplementary file).

### 3.4 Variability Between ROI Sizes

The feature selection model performance varied considerably across different ROI sizes. The best performance was obtained by the Var ROI size, as expected; the model failed to select any feature in the 1.6 ROI size dataset. Overall MSE values ranged from 33.15–36.22 in the train to 33.07–34.83 in the test set and  $R^2$  values ranged from 0.07–0.15 in the train set to 0.07–0.17 in the test dataset. Interestingly, model performance and feature selected in ROI size 1.0 and 1.2 datasets were similar to variable ROI size (Table 5). Furthermore, features selected in ROI size 1.0 and 1.2 datasets were more numerous than those in Var ROI size, but the type and class were similar.

Consistent and similar results were obtained with different feature selection models (MRMR and stepwise regression, in Table S2 of Supplementary file).

## 4 Discussion

This study established that feature extraction from the IM complex was feasible in 95% of cases for both RF and B-mode files. Approximately, 28% of the features were found to be stable across the three end-diastolic frames for all five ROI sizes. We further investigated the impact of frame and ROI size variability on extracted features using the feature selection technique. We found no impact on number, type and value of selected features due to frame variability. However, the ROI size did have an effect on the feature extraction, suggesting that the ROI size should be carefully chosen.

Radiomic analysis is increasingly utilized in carotid US, primarily for plaque analysis with findings typically derived from B-mode imaging [24]. This study is likely the first to apply radiomics in two novel ways: first, by focusing on the intima–media complex to characterize wall ultrastructure rather than solely on plaque; and second, by utilizing both B-mode images and raw radio-frequency signals, which contain richer spatial information than B-mode alone [26]. While the combined use of RF and B-mode US radiomic features has

**Table 1** Summary of Extracted Radiomic Features and their Classes

Feature Extraction Method	Feature Type	Feature Class	Total Number (n = count)	Features	
B-mode	First Order Features		7	Mean value Skewness Kurtosis Entropy Energy Median value Stand deviation	
		Higher Order Features (texture features)	4	Grey Level Distance Matrix (GLDM)	Mean entropy Entropy Contrast Angular second moment
			5	Neighboring Grey Level Dependence Matrix (NGLDM)	Coarseness Contrast Busyness Complexity Strength
		Grey Level Size Zone Matrix (GLSZM)	8	Small Zone Emphasis Large Zone Emphasis Gray-Level Non-uniformity Zone-Size Non-uniformity Zone Percentage Gray-Level Variance Zone-Size Variance Zone entropy	
		Grey Level Run Length Matrix (GLRLM)	8	Short Run Emphasis Long Run Emphasis Gray-Level Nonuniformity Run-Length Nonuniformity Run Percentage Gray-Level Variance Run-Length Variance Run entropy	
		Gray Level Dependence Matrix <sup>a</sup>	5	Small number emphasis (fitness index) large number emphasis (coarseness index) Number non-uniformity Entropy DCENT entropy	

**Table 1** (continued)

Feature Extraction Method	Feature Type	Feature Class	Total Number (n = count)	Features
Radio-frequency		Averaged features across 4 directions	10	Mean homogeneity Mean energy Mean local homogeneity Mean Autocorrelation Mean Correlation Mean Dissimilarity Mean sum average Mean entropy Mean Contrast Mean variance
	Wavelet Transform	Wavelet features	24	MeanVett 1–12 (Mean) SdVett 1–12 (standard deviation)
	Fractal Analysis	Fractal Analysis features	3	FD average FD standard deviation FD lacunarity
	Frequency domain	Spectral Features	12	spectral slope spectral Intercept Mid Band Fit S1 parameter S2 Parameter S3 Parameter S4 parameter signal power Spectral centroid Spectral Bandwidth spectral flatness Cress factor
	Time Domain Features	Time Series	5	Kurtosis cross zero count cross zero SD Peaks Fussy Entropy M parameter
	Nagakami distribution	Nagakami distribution mean diagram	1	First Order Features <sup>a</sup> Grey Level Distance Matrix <sup>a</sup> Grey Level Size Zone Matrix <sup>a</sup> Grey Level Run Length Matrix <sup>a</sup> Gray Level Dependence Matrix <sup>a</sup> Averaged features across 4 directions <sup>a</sup>
	Spatial Features	Skewness of spectrum difference Map	43	

**Table 1** (continued)

Feature Extraction Method	Feature Type	Feature Class	Total Number (n = count)	Features
		Direct Energy attenuation map	43	First Order Features <sup>a</sup> Grey Level Distance Matrix <sup>a</sup> Grey Level Size Zone Matrix <sup>a</sup> Grey Level Run Length Matrix <sup>a</sup> Gray Level Dependence Matrix <sup>a</sup> Averaged features across 4 directions <sup>a</sup>

Data are expressed as total number counts including both RF and B-mode based features (n = counts)

<sup>a</sup> Indicates the same set of features described in the B-mode feature family

**Table 2** Summary of baseline characteristics of the population

Variables	Missing data	Overall Population(n = 190)
Sex (Female) (n, %)	0	92 (48.4)
Smokers (n, %)	0	34 (17.8)
Diabetes (n, %)	0	37(19.4)
Hypertensive (n, %)	0	77(40.5)
Antidiabetic Drug Users (n, %)	1	21(11.05)
Antihypertensive Drug Users (n, %)	0	40(21.05)
Lipid Lowering Drug Users (n, %)	0	40(21.05)
Age (years)	0	59.5 ± 6.2
BMI (kg/m <sup>2</sup> )	0	25.2 ± 3.3
Mean Blood Pressure (mmHg)	0	94 ± 11
SBP (mmHg)	0	132 ± 18
DBP (mmHg)	0	76 ± 9
Heart Rate (bat/min)	0	64 ± 10
HDL (mg/dL)	0	59.1 ± 1 5.6
LDL (mg/dL)	0	142.9 ± 34.3
Cholesterol (mg/dL)	0	222.6 ± 38.4

Data for categorical variables are expressed as total number counts (n = counts) and percentage of total and for continuous variables as Mean ± SD (standard deviation)

**Table 3** Summary of carotid geometric and mechanical characteristics

Carotid Variables	Missing data	Overall Population(n = 190)
Presence of carotid Plaque (n, %)	0	30 (15.7)
Distension (µm)	3	359.88 ± 121
External diastolic Diameter (mm)	0	7.17 ± 0.73
Compliance (m <sup>2</sup> /kPa)	3	0.58 ± 0.23
Distensibility coefficient (kPa-1*10 <sup>-3</sup> )	3	21.43 ± 8.63
Carotid Pulse Wave velocity (m/s)	3	7.47 ± 1.57
IMT (um)	0	631 ± 108.6

Data for categorical variables are expressed as total number counts (n = counts) and percentage of total and for continuous variables as Mean ± SD (standard deviation)

been applied in oncology, its application in cardiovascular radiomics remains unexplored. Incorporating RF-based radiomic features has improved accuracy in cancer detection and characterization compared to B-mode alone in breast cancer [50, 51].

The main objective of our study was to assess the feasibility and reproducibility of extracting radiomic features from the IM complex using both RF and B-mode US data. In terms of feasibility, RF and B-mode feature extraction was successfully performed on 190 out of 200 clips. The only clips where feature extraction was

**Table 4** Results of reproducibility of features across frames

Frame No	Roi size (mm)	Model	Train MSE	Train R <sup>2</sup>	Test MSE	Test R <sup>2</sup>	Feature selected	Feature Name (Feature class)	Feature Type
1	Var	Lasso L1	34.36	0.09	40.28	0.05	4	Busyness and complexity (NGLDM), Gray-Level Nonuniformity (GLRLM), SdVett_5 (Wavelet transform)	B-mode higher order and Wavelet transform
2	Var	Lasso L1	32.31	0.14	38.31	0.13	10	Standard Deviation (First order), Entropy (GLDM), Contrast (NGTDM), Mean entropy (Avg features), Gray-Level Variance (GLRLM), meanVett_3, SdVett_5, SdVett_9 (Wavelet transform), and RF First order: Median (DEA) and Median (SSD)	B-mode first order, higher order, wavelet and RF first order
3	Var	Lasso L1	33.73	0.112	42.32	0.11	2	Gray-Level Nonuniformity (GLRLM), SdVett_9(Wavelet transform)	B- mode Higher order and Wavelet transform
Med	Var	Lasso L1	33.86	0.13	30.79	0.11	3	Complexity (NGTDM), Gray-Level Nonuniformity (GLRLM), SdVett_9 (Wavelet transform)	B- mode Higher order and Wavelet transform

Dependent Variable: Chronological age. The Mean square Error (MSE) is represented in years

DEA Direct Energy attenuation map, GLDM Grey Level Distance Matrix, GLRLM Grey Level Run Length Matrix, NGLDM Neighboring Grey Level Dependence Matrix, SSD Skewness of spectrum difference Map

not feasible were those in which the IMT was not visible at all.

Once feasibility was established, we investigated issues related to ROI delineation, which is crucial for feature extraction integrity. Indeed, inaccurate ROI delineation could lead to incomplete or inaccurate representation of the target anatomical structure (IM complex). In particular, we investigated the impact of the cardiac cycle frame (temporal aspect) and of the size of the region of interest (spatial aspect) on the radiomic features.

First, our analysis of frame variability sought to recognize stable and reproducible features across 3 end-diastolic frames. By intraclass correlation coefficient, we identified a robust set of features consistently present irrespective of the frame and ROI size (from B-mode first-order, higher-order, wavelet, RF first-order, and time series classes).

We further investigated the impact of frame variability on feature selection using chronological age as an outcome. The consistent selection of the same feature types across all frames (type of features) indicated that the choice of frame does not significantly impact the analysis, allowing for flexibility in frame selection without compromising the integrity of the results. The selected features from B-mode first-order features describe intensity and contrast, reflecting IM complex density. Higher-order features reveal texture and heterogeneity,

indicating tissue structure. Wavelet features capture multi-scale structural changes, detecting alterations in the IM complex [52]. RF features provide insights into acoustic properties, revealing tissue mechanical characteristics [33, 53, 54].

Second, we evaluated whether a fixed, automatically chosen, ROI size could provide results similar compared to a tailored ROI size manually drawn by an operator. Our results show that fixed ROI sizes of 1.0 or 1.2 mm, but not 1.4 and 1.6 mm, provide similar results in terms of feature reproducibility and selection compared to the variable ROI. This suggests that the choice of ROI size is critical in optimizing the extraction of relevant features, highlighting the importance of selecting an appropriate size tailored to the anatomical characteristics of the IM complex. Inclusion of portions of the adventitia in the ROI significantly alter the radiomic feature profile.

Utilizing this methodological pipeline for predictive modelling may offer the potential to capture both atherosclerotic and arteriosclerotic features (biomarkers) using a single, non-invasive CCA ultrasound. As vascular ageing involves both atherosclerotic and arteriosclerotic processes, radiomic analysis may aid in the early detection of vascular ageing, contribute to improved risk stratification for vascular diseases, and provide additional insights into carotid wall ultrastructure, potentially supporting timely interventions to reduce adverse outcomes.

**Table 5** Results of variability between ROI sizes

Median	ROI size	Model	Train MSE	Train R <sup>2</sup>	Test MSE	Test R <sup>2</sup>	Feature Selected	Feature Name (Feature class)	Feature Type
Med	Var	Lasso	33.86	0.13	30.79	0.17	3	Complexity (NGLDM), Gray-Level Nonuniformity (GLRLM), SdVett_9 (Wavelet transform)	B-mode higher order and Wavelet transform
Med	1	Lasso	33.15	0.15	33.07	0.11	5	Coarseness (NGTDM), Mean Correlation (Avg features), Run length Non-uniformity (GLRLM), meanVett_3 (Wavelet transform), and RF First order: Standard deviation (DEA)	B-mode higher order, Wavelet transform and Rf first order
Med	1.2	Lasso	33.24	0.14	31.87	0.15	6	Entropy (First order), Coarseness (NGTDM), Mean variance (Avg features), SdVett_1 and SdVett_9 (Wavelet transform) and RF first order: Standard deviation (DEA)	B-mode first, higher order, Wavelet transform and Rf first order
Med	1.4	Lasso	36.22	0.07	34.83	0.07	3	Skewness (first order), Coarseness (NGTDM), Gray level non-uniformity (GLRLM)	B-mode first and higher order
Med	1.6	Lasso	–	–	–	–	0	–	–

Dependent Variable: Chronological age. The Mean square Error (MSE) is represented in years

DEA Direct Energy attenuation map, GLDM Grey Level Distance Matrix, GLRLM Grey Level Run Length Matrix, NGLDM Neighboring Grey Level Dependence Matrix, SSD Skewness of spectrum difference Map

We acknowledge some limitations in this study. First, since this is a pilot investigation, it was conducted in a small highly selected population sample. We plan to validate our findings in an external dataset that includes a broader age range and diverse ethnicities. Second, feature extraction has been performed only in end-diastolic frames: exploring the potential impact of different cardiac cycle phases on feature extraction could provide additional insights. Third, the current study is not powered for predictive modelling, but only to investigate the robustness of the approach. Further validation and refinement, particularly with a larger dataset, are needed before making definitive conclusions about its effectiveness. Fourth, clinical relevance of the extracted features as well as potential confounding factors such as comorbidities, lifestyle factors and environmental exposures is beyond the scope of this article, but needs to be investigated in future studies.

### 5 Conclusions

Our study demonstrates the feasibility of radiomic US feature extraction from the IM complex using both RF and B-mode US data, showing minimal sensitivity to variations in frame selection. However, ROI size significantly affects feature extraction, highlighting the importance of precise ROI delineation in radiomics research. Building on these methodological improvements, we aim to expand radiomics applications in vascular health as novel biomarkers of vascular ageing.

### Abbreviations

CAC	Calcium score
CT	Computed tomography
EVA	Early vascular ageing
ICC	Intraclass correlation
IM	Intima-media
IMT	Intima-media thickness
LASSO	Least absolute shrinkage and selection operator
MRI	Magnetic resonance imaging
MRMR	Minimum redundancy maximum relevance
MSE	Mean square error
PWV	Pulse wave velocity
PPS3	Paris Prospective Study III
RF	Radio frequency
ROI	Region of interest
SD	Standard deviation
SUPERNOVA	Supernormal vascular ageing
T2D	Type 2 diabetes
US	Ultrasound
VAR	Variable

### Supplementary Information

The online version contains supplementary material available at <https://doi.org/10.1007/s44200-025-00076-w>.

Below is the link to the electronic supplementary material. Supplementary file1 (DOCX 25 KB)

### Author Contributions

MJ design and development of GUI, methodology, data analysis, interpretation of data and drafting the manuscript. FP, EB, FF worked on the design and development of the GUI, interpretation of data and critical review of the manuscript. HK data collection physician for PPS III study. XJ, JP conception, design and development of the PPS III study. PB, JP, RM conception of the research, interpretation of results and critical review of the manuscript.

### Funding

This work was supported by a research grant from the European Commission Marie Skłodowska-Curie Actions PhD program: MINDSHIFT (grant number 954798, website: <http://www.eumindshift.eu>). The PPS3 (Paris Prospective Study III) was supported by grants from The National Research Agency (ANR), the Research Foundation for Hypertension (FRHTA), the Research Institute in Public Health (IRESP) and the Region Ile de France (Domaine d'Intérêt Majeur) and the H2020 ESCAPENET research program.

### Availability of Data and Materials

The data used in the current study are not publicly available due privacy issues but it will be made available on reasonable request. All data analyzed in this study are presented within the paper and supplementary material.

### Declarations

#### Ethics Approval and Consent to Participate

The study protocol was approved by the Ethics Committee of Cochin Hospital (Paris, France) and was registered on the World Health Organization International Clinical Trials Registry platform (NCT00741728) on 08/25/2008. A total of 10,157 men and women underwent a comprehensive preventive medical checkup, after signing an informed consent form.

#### Consent for Publication

All authors read and approved the final manuscript for publication.

#### Competing of Interests

The authors declare no competing interests.

#### Author details

<sup>1</sup>Université Paris Cité, Inserm, PARCC, F-75015 Paris, France. <sup>2</sup>Clinical Pharmacology Unit, AP-HP, Hôpital Européen Georges Pompidou, F-75015 Paris, France. <sup>3</sup>Institute of Clinical Physiology, Italian National Research Council (CNR), Pisa, Italy.

Received: 27 September 2024 Accepted: 10 March 2025

Published online: 31 March 2025

### References

- Boutouyrie P, Chowienczyk P, Humphrey JD, Mitchell GF. Arterial stiffness and cardiovascular risk in hypertension. *Circ Res*. 2021;128(7):864–86.
- Laurent S. Defining vascular aging and cardiovascular risk. *J Hypertens*. 2012;30:S3–8.
- Nilsson PM, Boutouyrie P, Laurent S. Vascular aging: a tale of EVA and ADAM in cardiovascular risk assessment and prevention. *Hypertension*. 2009;54(1):3–10.
- Nilsson MP. Early vascular ageing a concept in development. *Eur Endocrinol*. 2015;11(1):26–31.
- Bruno RM, Nilsson PM, Engström G, Wadström BN, Empana JP, Boutouyrie P, et al. Early and supernormal vascular aging: clinical characteristics and association with incident cardiovascular events. *Hypertension*. 2020;76(5):1616–24.
- Laurent S, Boutouyrie P, Cunha PG, Lacolley P, Nilsson PM. Concept of extremes in vascular aging: from early vascular aging to supernormal vascular aging. *Hypertension*. 2019;74(2):218–28.
- Li A, Yan J, Zhao Y, Yu Z, Tian S, Khan AH, et al. Vascular aging: assessment and intervention. *CIA*. 2023;18:1373–95.
- Jamthikar AD, Gupta D, Saba L, Khanna NN, Viskovic K, Mavrogeni S, et al. Artificial intelligence framework for predictive cardiovascular and stroke risk assessment models: a narrative review of integrated approaches using carotid ultrasound. *Comput Biol Med*. 2020;126:104043.
- Mantella LE, Colledanchise KN, Héту MF, Feinstein SB, Abunassar J, Johri AM. Carotid intraplaque neovascularization predicts coronary artery disease and cardiovascular events. *Eur Heart J Cardiovasc Imaging*. 2019;20(11):1239–47.
- Sillescu H, Sartori S, Sandholt B, Baber U, Mehran R, Fuster V. Carotid plaque thickness and carotid plaque burden predict future cardiovascular events in asymptomatic adult Americans. *Eur Heart J Cardiovasc Imaging*. 2018;19(9):1042–50.
- Vasan RS, Pan S, Xanthakis V, Beiser A, Larson MG, Seshadri S, et al. Arterial stiffness and long-term risk of health outcomes: the framingham heart study. *Hypertension*. 2022;79(5):1045–56.
- Van Sloten TT, Sedaghat S, Laurent S, London GM, Pannier B, Ikram MA, et al. Carotid stiffness is associated with incident stroke. *J Am Coll Cardiol*. 2015;66(19):2116–25.
- Willeit P, Tschiderer L, Allara E, Reuber K, Seekircher L, Gao L, et al. Carotid intima-media thickness progression as surrogate marker for cardiovascular risk: meta-analysis of 119 clinical trials involving 100 667 patients. *Circulation*. 2020;142(7):621–42.
- Yeboah J, McClelland RL, Polonsky TS, Burke GL, Sibley CT, O'Leary D, et al. Comparison of novel risk markers for improvement in cardiovascular risk assessment in intermediate-risk individuals. *JAMA*. 2012;308(8):788.
- Reesink KD, Spronck B. Constitutive interpretation of arterial stiffness in clinical studies: a methodological review. *Am J Physiol-Heart Circ Physiol*. 2019;316(3):H693–709.
- Rogers W, Thulasi Seetha S, Refaee TAG, Lieverse RIV, Granzier RWY, Ibrahim A, et al. Radiomics: from qualitative to quantitative imaging. *Br J Radiol*. 2020;93(1108):20190948.
- Van Griethuysen JJM, Lambregts DMJ, Trebeschi S, Lahaye MJ, Bakers FCH, Vliegen RFA, et al. Radiomics performs comparable to morphologic assessment by expert radiologists for prediction of response to neoadjuvant chemoradiotherapy on baseline staging MRI in rectal cancer. *Abdom Radiol*. 2020;45(3):632–43.
- Wang J, Yu X, Zeng J, Li H, Qin P. Radiomics model for preoperative prediction of 3-year survival-based CT image biomarkers in esophageal cancer. *Eur Arch Otorhinolaryngol*. 2022;279(11):5433–43.
- Tsarouchi MI, Vlachopoulos GF, Karahaliou AN, Vassiou KG, Costaridou LI. Multi-parametric MRI lesion heterogeneity biomarkers for breast cancer diagnosis. *Physica Med*. 2020;80:101–10.
- Bhardwaj D, Dasgupta A, DiCenzo D, Brade S, Fatima K, Quaiok K, et al. Early changes in quantitative ultrasound imaging parameters during neoadjuvant chemotherapy to predict recurrence in patients with locally advanced breast cancer. *Cancers*. 2022;14(5):1247.
- Cui Y, Wang G, Ren J, Hou L, Li D, Wen Q, et al. Radiomics features at multiparametric MRI predict disease-free survival in patients with locally advanced rectal cancer. *Acad Radiol*. 2022;29(8):e128–38.
- Cheng X, Dong Z, Liu J, Li H, Zhou C, Zhang F, et al. Prediction of carotid in-stent restenosis by computed tomography angiography carotid plaque-based radiomics. *JCM*. 2022;11(11):3234.
- Dong Z, Zhou C, Li H, Shi J, Liu J, Liu Q, et al. Radiomics versus conventional assessment to identify symptomatic participants at carotid computed tomography angiography. *Cerebrovasc Dis*. 2022;51(5):647–54.
- Hou C, Li S, Zheng S, Liu LP, Nie F, Zhang W, et al. Quality assessment of radiomics models in carotid plaque: a systematic review. *Quant Imaging Med Surg*. 2024;14(1):1141–54.
- Huang Z, Cheng XQ, Liu HY, Bi XJ, Liu YN, Lv WZ, et al. Relation of carotid plaque features detected with ultrasonography-based radiomics to clinical symptoms. *Transl Stroke Res*. 2022;13(6):970–82.
- Le EPV, Rundo L, Tarkin JM, Evans NR, Chowdhury MM, Coughlin PA, et al. Assessing robustness of carotid artery CT angiography radiomics in the identification of culprit lesions in cerebrovascular events. *Sci Rep*. 2021;11(1):3499.
- Liu Y, Kong Y, Yan Y, Hui P. Explore the value of carotid ultrasound radiomics nomogram in predicting ischemic stroke risk in patients with type 2 diabetes mellitus. *Front Endocrinol*. 2024;19(15):1357580.
- Van Engelen A, Wannarong T, Parraga G, Niessen WJ, Fenster A, Spence JD, et al. Three-dimensional carotid ultrasound plaque texture predicts vascular events. *Stroke*. 2014;45(9):2695–701.
- Molinari F, Zeng G, Suri JS. A state of the art review on intima-media thickness (IMT) measurement and wall segmentation techniques for carotid ultrasound. *Comput Methods Programs Biomed*. 2010;100(3):201–21.
- Scicolone R, Vacca S, Pisu F, Benson JC, Nardi V, Lanzino G, et al. Radiomics and artificial intelligence: general notions and applications in the carotid vulnerable plaque. *Eur J Radiol*. 2024;176:111497.

31. Ricci V, Cocco G, Donati D, Fari G, Chang KV, Özçakar L. From histopathology to high-resolution ultrasound imaging of skin scars. *Diagnostics*. 2023;13(24):3629.
32. Lacolley P, Regnault V, Segers P, Laurent S. Vascular smooth muscle cells and arterial stiffening: relevance in development, aging, and disease. *Physiol Rev*. 2017;97(4):1555–617.
33. Hu R, Singla R, Deeba F, Rohling RN. Acoustic shadow detection: study and statistics of B-mode and radiofrequency data. *Ultrasound Med Biol*. 2019;45(8):2248–57.
34. on behalf of the PPS3 Study Group, Empana JP, Bean K, Guibout C, Thomas F, Bingham A, et al. Paris prospective study III: a study of novel heart rate parameters, baroreflex sensitivity and risk of sudden death. *Eur J Epidemiol*. 2011;26(11):887–92.
35. Standard B-mode ultrasound measures local carotid artery characteristics as reliably as radiofrequency phase tracking in symptomatic carotid artery patients - Ultrasound in medicine and biology [Internet]. [cited 2024 Aug 21]. Available from: [https://www.umbjournal.org/article/S0301-5629\(15\)00476-7/abstract](https://www.umbjournal.org/article/S0301-5629(15)00476-7/abstract)
36. Ariyoshi K, Okuya S, Kunitsugu I, Matsunaga K, Nagao Y, Nomiya R, et al. Ultrasound analysis of gray-scale median value of carotid plaques is a useful reference index for cerebro-cardiovascular events in patients with type 2 diabetes. *J Diabetes Invest*. 2015;6(1):91–7.
37. Sim Y, Lee SE, Kim EK, Kim S. A radiomics approach for the classification of fibroepithelial lesions on breast ultrasonography. *Ultrasound Med Biol*. 2020;46(5):1133–41.
38. Allison JW, Barr LL, Massoth RJ, Berg GP, Krasner BH, Garra BS. Understanding the process of quantitative ultrasonic tissue characterization. *Radiographics*. 1994;14(5):1099–108.
39. Kim JK, Park HW. Statistical textural features for detection of microcalcifications in digitized mammograms. *IEEE Trans Med Imaging*. 1999;18(3):231–8.
40. Arivazhagan S, Ganesan L. Texture classification using wavelet transform. *Pattern Recogn Lett*. 2003;24(9–10):1513–21.
41. Al-Kadi OS, Watson D. Texture analysis of aggressive and nonaggressive lung tumor CE CT images. *IEEE Trans Biomed Eng*. 2008;55(7):1822–30.
42. Alic L, Niessen WJ, Veenland JF. Quantification of heterogeneity as a biomarker in tumor imaging: a systematic review. *PLoS ONE*. 2014;9(10):e110300.
43. Van Griethuysen JJM, Fedorov A, Parmar C, Hosny A, Aucoin N, Narayan V, et al. Computational radiomics system to decode the radiographic phenotype. *Can Res*. 2017;77(21):e104–7.
44. Zheng Q, Lin C, Xu D, Zhao H, Song M, Ou D, et al. A preliminary study on exploring a potential ultrasound method for predicting cervical cancer. *J Cancer*. 2022;13(3):793–9.
45. Xiao T, Shen W, Wang Q, Wu G, Yu J, Cui L. The detection of prostate cancer based on ultrasound RF signal. *Front Oncol*. 2022;12(12):946965.
46. Shams E, Karimi D, Moussavi Z. Bispectral analysis of tracheal breath sounds for Obstructive Sleep Apnea. In: 2012 annual international conference of the IEEE engineering in medicine and biology society [Internet]. San Diego, CA: IEEE; 2012 [cited 2024 Feb 12]. p. 37–40. Available from: <http://ieeexplore.ieee.org/document/6345865/>
47. Tsui PH, Zhou Z, Lin YH, Hung CM, Chung SJ, Wan YL. Effect of ultrasound frequency on the Nakagami statistics of human liver tissues. *PLoS ONE*. 2017;12(8):e0181789.
48. Wang Q, Dong Y, Xiao T, Zhang S, Yu J, Li L, et al. Prediction of programmed cell death protein 1 in hepatocellular carcinoma patients using radiomics analysis with radiofrequency-based ultrasound multifeature maps. *BioMed Eng OnLine*. 2022;21(1):24.
49. Tibshirani R. Regression shrinkage and selection via the lasso. *J R Stat Soc Ser B Stat Methodol*. 1996;58(1):267–88.
50. Klimonda Z, Karwat P, Dobruch-Sobczak K, Piotrkowska-Wróblewska H, Litniewski J. Assessment of breast cancer response to neoadjuvant chemotherapy based on ultrasound backscattering envelope statistics. *Med Phys*. 2022;49(2):1047–54.
51. Tadayyon H, Sannachi L, Gangeh MJ, Kim C, Ghandi S, Trudeau M, et al. A priori prediction of neoadjuvant chemotherapy response and survival in breast cancer patients using quantitative ultrasound. *Sci Rep*. 2017;7(1):45733.
52. Golemati S, Lehareas S, Tsiaparas NN, Chatziioannou A, Nikita KS, Perrea DN. Multiresolution features of carotid artery wall and plaque toward identifying vulnerable asymptomatic cases from B-mode ultrasound. In: 2013 IEEE international ultrasonics symposium (IUS) [Internet]. Prague, Czech Republic: IEEE; 2013 [cited 2024 Jul 17]. p. 872–5. Available from: <http://ieeexplore.ieee.org/document/6725296/>
53. Dong Y, Wang QM, Li Q, Li LY, Zhang Q, Yao Z, et al. Preoperative prediction of microvascular invasion of hepatocellular carcinoma: radiomics algorithm based on ultrasound original radio frequency signals. *Front Oncol*. 2019;14(9):1203.
54. Azzopardi C, Camilleri KP, Hicks YA. Carotid ultrasound segmentation using radio-frequency derived phase information and gabor filters. In: 2015 37th annual international conference of the IEEE engineering in medicine and biology society (EMBC) [Internet]. Milan: IEEE; 2015 [cited 2024 May 2]. p. 6338–41. Available from: <http://ieeexplore.ieee.org/document/7319842/>

## Publisher's Note

Springer Nature remains neutral with regard to jurisdictional claims in published maps and institutional affiliations.